Supplemental Material

Supplementary Information (SI)

for

Large fraction of winter precipitation variability in two major Himalayan basins explained by Atmospheric Rivers

Rosa Vellosa Lyngwa[1], Waqar Ul Hasssan[1], Munir Ahmad Nayak[2*], Mohd. Farooq Azam[1]

[1]*Department of Civil Engineering, Indian Institute of Technology Indore, Simrol, Indore, Madhya Pradesh, India*

[2]**Department of Civil Engineering, National Institute of Technology Srinagar, Hazratbal, Jammu and Kashmir, India.*

Correspondence to: Munir Ahmad Nayak, Department of Civil Engineering, National Institute of Technology Srinagar, Hazratbal, Jammu and Kashmir, India-190006.munir.nayak@nitsri.net

Contents:

1. Details of ARs in mid-June 2013 and early Sept 2014

Two Category 5 ARs during mid-June 2013 and early Sept 2014 were observed in northern India, Himalayas. The ARs struck Jammu & Kashmir on 3rd Sept 2014 and Uttarakhand on 12th June 2013, respectively. The AR in Sept 2014 lasted for 3 days from 3rd-5th Sept (Figures 1a and S1a, showed 3rd-Sept 2014, 18:00 UTC) and in 2013 the AR stalled for about 7 days from 12th-18th June and reached peak intensity on 16th and 17th June (Figure 1b, S1b; showed16 June, 18:00 UTC). Orographic lift of AR moisture resulted in heavy precipitation in the surrounding areas, which translated into the most disastrous floods in Northern India.

Figure S1: Illustrating the AR-link to high precipitation and flood events.

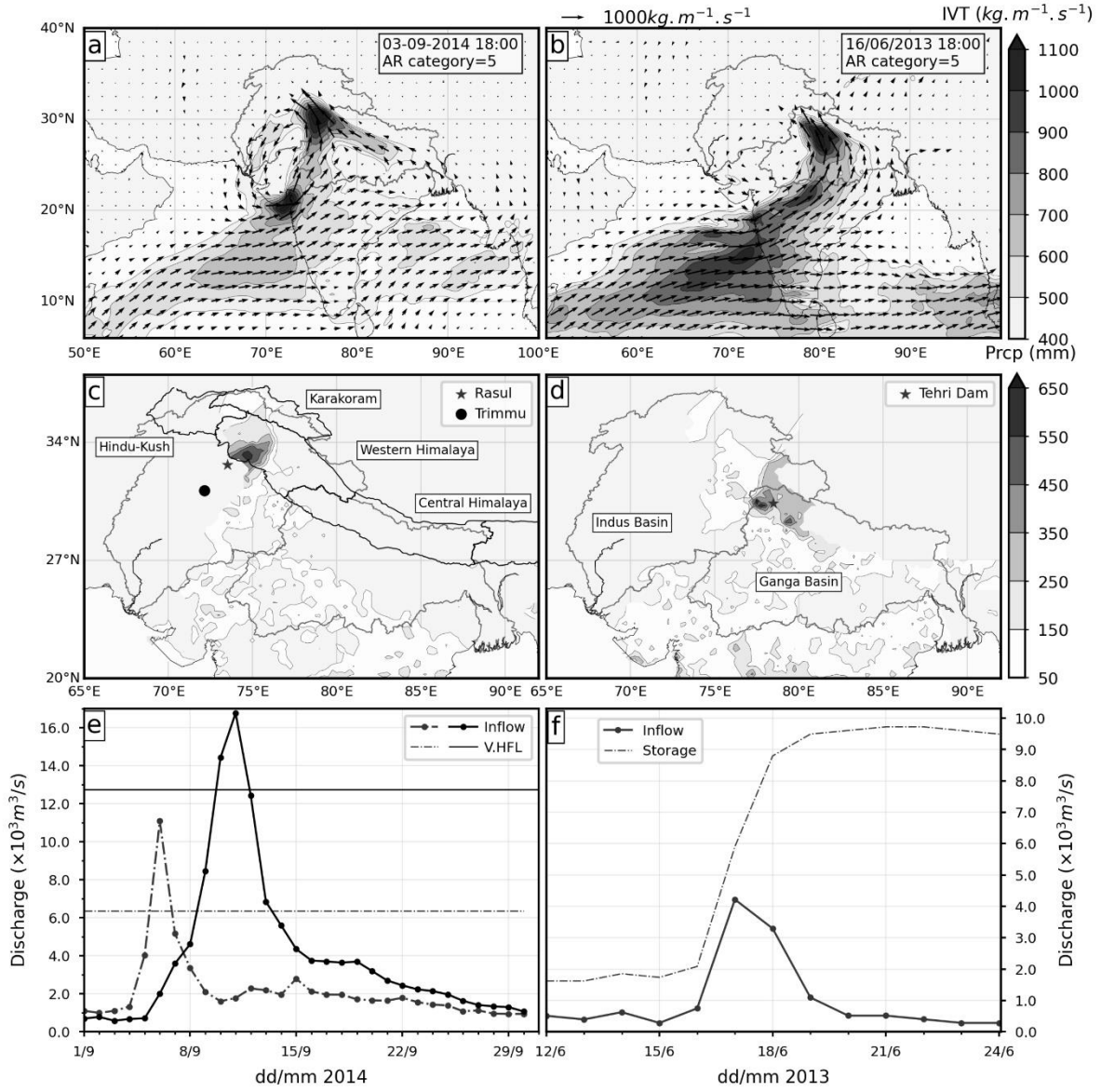

Figure S1: Similar to Figure 1, except for (c) and (d) in which IMD is used for precipitation. IVT ($kg.m^{-1}.s^{-1}$) on (a) 3rd Sept 2014 at 18:00 UTC and (b) 16th June 2013 at 18:00 UTC; (c) and (d) show the total accumulated precipitation (mm) during the events. The star and circle (solid) represent the discharge measuring stations in Jhelum River and Chenab River respectively in (c), and the star in (d) represents the location of the Tehri dam at Bhagirathi River. (e) and (f) show discharge at the gauge stations in (c) for September 2014, and storage in (d) for June 2013; In (e) the discharge and very high flood level are shown by solid for at Rasul and by dashed lines for Trimmu in IB (Indus Basin), and in (f) the discharges are shown by solid line and storage by dashed line at Tehri dam in GB (Ganga Basin).

Text S1: Precipitation during the two AR events.

IMD showed similar spatial patterns for rainfall as compared to WFDE5, except in the upper reached of IB, and showed much higher rainfall accumulations near the gauge stations (Figure S1c). IMD showed the rainfall magnitude 200 mm higher than that observed by WFDE5, which could be due to the lack of ground-based information used for bias correction and low resolution of WFDE5.

From 2nd−6th Sept 2014, Western Himalaya (WH) received precipitation greater than 450 mm precipitation (~32% of annual precipitation (Figure S1c)), nearly 550 mm in Kashmir generated surplus streamflow in Jhelum and Chenab Rivers. In June 2013, Uttarakhand received greater than 350 mm precipitation ($\sim 28\%$ of annual precipitation) during 12th–18th June 2013.

Text S2: Summary of the Algorithm:

1. At each grid, 6-hourly IVTs are computed in the study region for the period $1982 - 2018$.
2. IVT thresholds are computed for each calendar day as the local 85th percentile value of the IVT distribution for that calendar day at every grid.
3. To identify ARs that penetrate the Himalayas, a detection transect is then defined along the foothills of the Himalayas.
4. The transect is split into 5 bins (A to E) considering the large IVT variations along its length (due to latitude changes). Bin thresholds are then computed as spatial average of grid thresholds within the bin.
5. At a timestep, the maximum IVT grid is identified on the transect and anchored as the first grid of the axis if its IVT surpasses the respective bin threshold (Steps 1 & 2).
6. Among three adjacent grids in the west of the first grid, the grid with maximum IVT is anchored as the second grid if it surpasses the grid's threshold.

7. Step 6 is repeated to find subsequent grids forming the axis until the maximum IVT of the adjacent grid is below the threshold.
8. Similarly, the grids forming the potential AR-axis are searched southward.
9. The axes obtained from step 8 are screened for the minimum length requirement of ARs, and presence of cyclones (i.e., AR timesteps that match the cyclone timesteps).
10. Only persistent AR events that last longer than 18 hours are retained. An AR event is defined as a group of consecutive AR timesteps.
11. Lastly, the two sets of AR events are reviewed for unique events, i.e., if the events from the two sets have at least one timestep in common, the event with the largest average IVT is taken as the AR.

Figure S3: The 80th percentile precipitation using IMD.

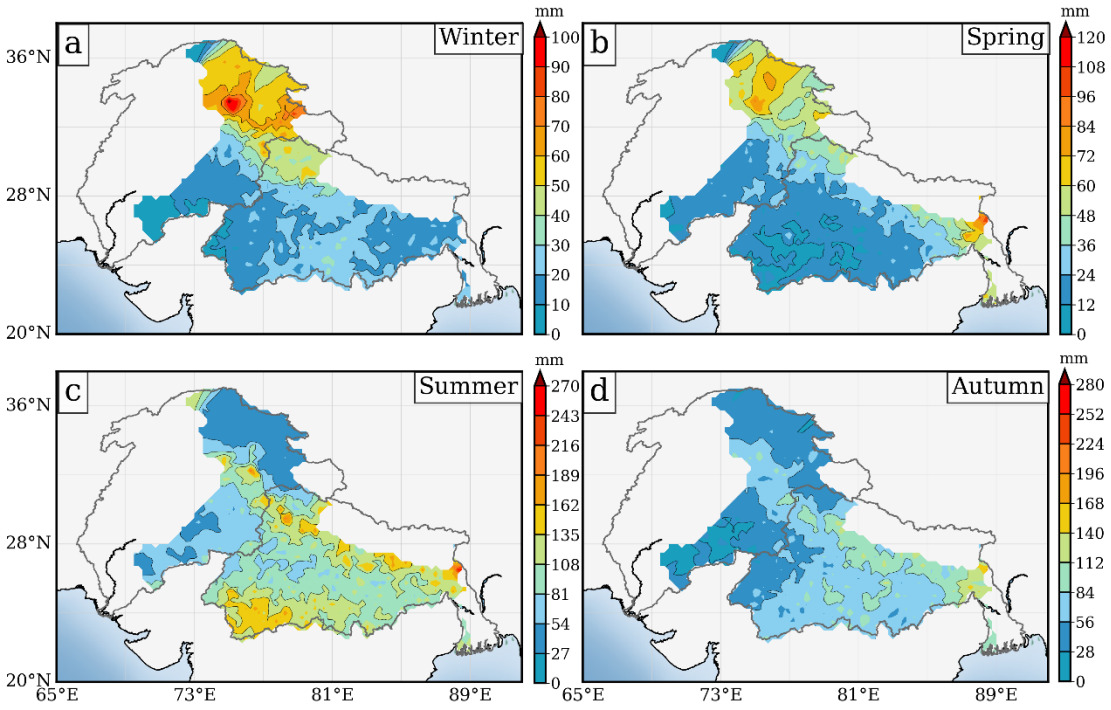

Figure S3: The 80th percentile for (a) winter (b) spring (c) summer and (d) autumn seasons for Indian IB and GB, using IMD (1982 – 2018).

Figure S4: Difference between IMD and WFDE5 80th percentile:

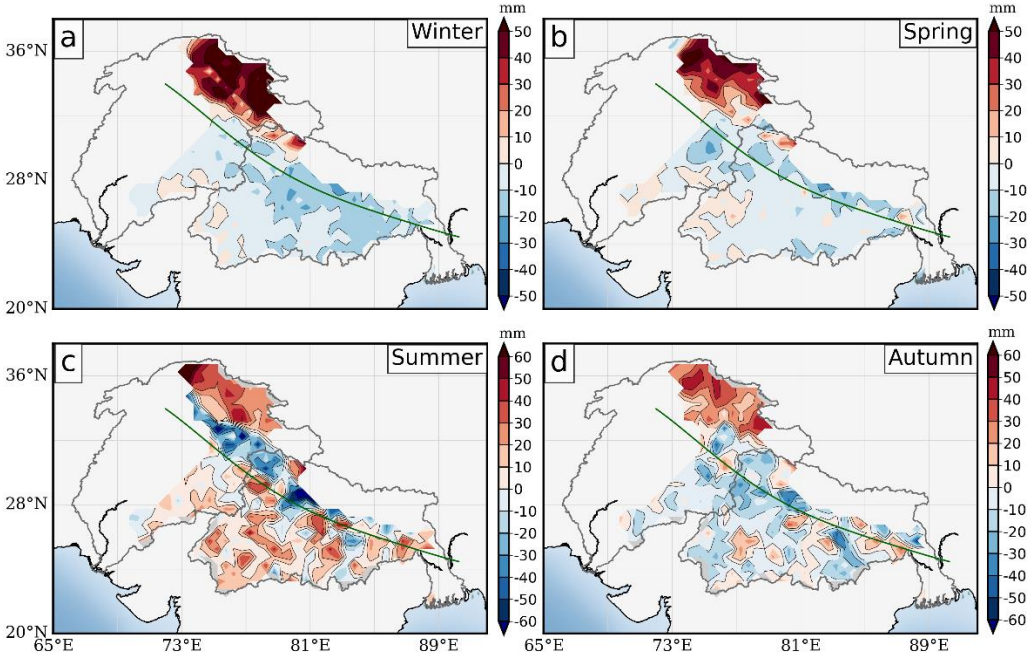

Figure S4: Difference between IMD and WFDE5 80th percentile when the base period is same i.e., 1982-2016, and when the periods are different i.e., IMD (1982-2018) and WFDE5 (1982-2016) we observed no appreciable changes (Figure not shown). The differences were computed at 0.5° × 0.5.

Figure S5: AR contribution to seasonal precipitation extreme using WFDE5.

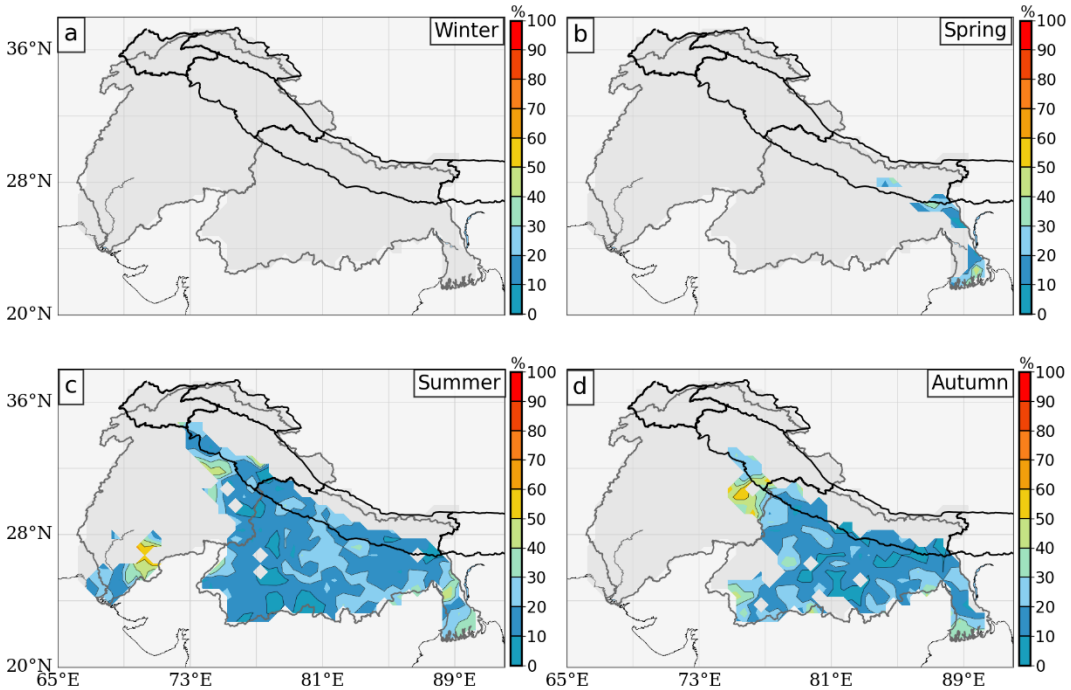

Figure S5a: Same as Figure 5 but using WFDE5. The criteria for precipitation maxima are (a) above 60 mm for the daily precipitation maxima and (b) each grid cell should have at least 7 years of their seasonal maxima (greater than 60 mm). Grey color within the basins shows the grid cells that do not satisfy the criteria.

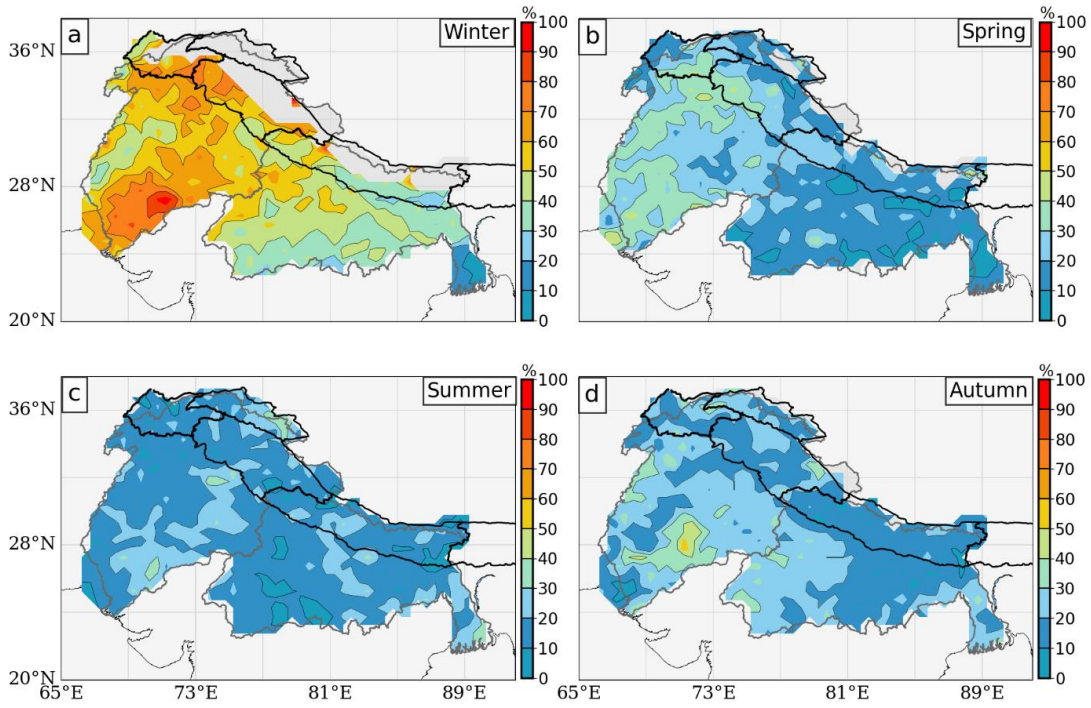

Figure S5b: Relative frequency of seasonal rainfall maxima (in %) related to ARs for 1982 – 2016 using WFDE5. (a) for winter, (b) spring, (c) summer, and (d) autumn seasons. The grids shaded in dark gray have either seasonal maximum precipitation less than 2mm or the number of seasonal maxima is less than 7."

Text S5: Sensitivity of AR contribution to thresholds.

In order to assess the sensitivity of AR contributions to the threshold for daily maxima, we used a lower threshold of 2 mm (instead of 40 mm) (Figure S5b). The results highlight that ARs contributed mostly between 30 – 90% (for comparison, the contribution is 50 – 100% based on 40mm threshold; Figure 5) of the winter rainfall extremes in the Indus and Ganga basins; up to 50% (up to 60%, Figure 5) of the extremes in spring are related to ARs, particularly in Indus basin; and 20 – 50% (20 – 50%, Figure 5) of the extremes in summer and autumn are AR-related in both basins. Based on the two thresholds (2 mm and 40 mm), we find minor differences in the fractional AR contributions to extremes. Moreover, ARs contribute to "daily maxima" throughout the year; however, winter ARs have more contribution to the extreme precipitation highlighting that ARs are relevant to both small and large daily maxima at regional scale."

Figure S6: Average AR contribution to total and seasonal rainfall using IMD.

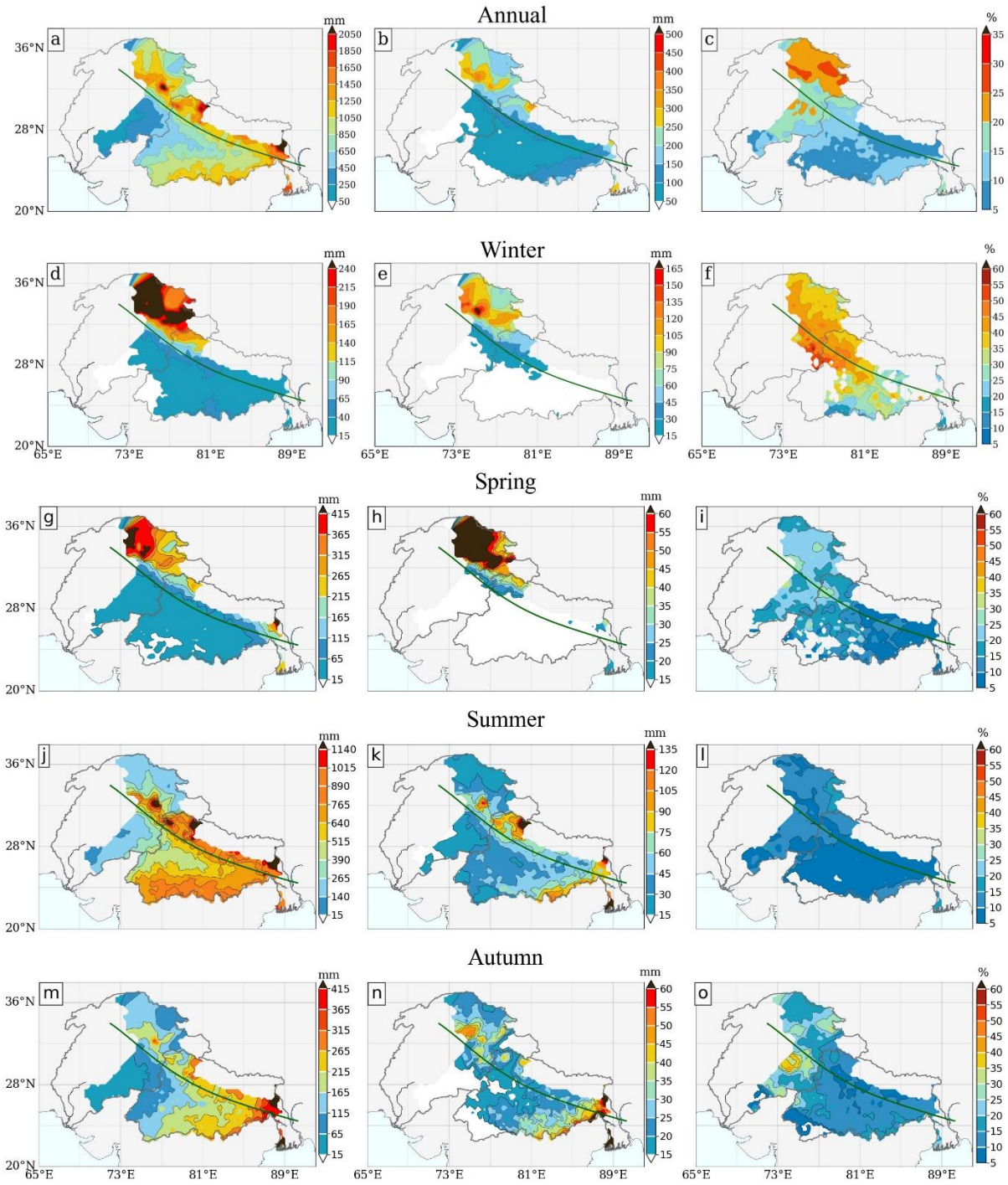

Figure S6: Similar to Figure 2, but using rainfall data from IMD for the period 1982 – 2018 [Dates in AR Database are in UTC and IMD are in IST].

Text S6: Average AR contribution to total and seasonal rainfall using IMD:

Figure S6 shows the IMD annual average rainfall patterns resemble WFDE5 observations closely in magnitude over both basins except north IB, with precipitation highly

underestimated by WFDE5. The maximum rainfall location matches well in both the cases; however, there are large differences between the two in representing spatial patterns of rainfall for these basins, especially for northern Indian IB. As described in the Data section that WDFE5 is a reanalysis data (i.e., it uses a combination of observations and model outputs) that may be associated with systematic model errors, and IMD is developed from gauge stations observations which are interpolated into gridded data. However, it is to be noted that only a handful of stations are present in lower elevated areas of north India, and the observations from these gauge data are interpolated to extent up to the northern border of India (Pai & Bhan, 2014; Rajeevan et al., 2006). Seasonally, the highest rainfall is observed in summer, followed by autumn and spring (Figures S6 g, j and m).

We observed that ARs contribute $20-35\%$ in northern IB, and $5-20\%$ in southern IB (for rainfall of $100-300$ mm/year. For GB, ARs contribute $5-15\%$ of annual rainfall in nearly the entire basin and $\sim 25\%$ is found for grid cells in the northern most reaches (Figure S6c). In winter, the average AR-related rainfall between $60-165$ mm/winter (figure S6e) is observed in northern IB and northwest GB (Uttarakhand), predominantly over mountain regions. ARs contribute between $40-50\%$ to winter rainfall in northern IB (WH) and upper GB (west of central Himalaya (CH)), and $20-40\%$ in south GB (Figure S6f). These observations show similar relative contribution of ARs as observed using WFDE5, except for regions in the northmost IB. In summer, ARs contribute mainly 15% to the rainfall in IB though 10% and 20% are also observed in south and northern IB. In GB, ARs contribute between $10-15\%$ of the seasonal summer precipitation ($500-1125$ mm/summer) in the mountains and southern GB (Figures S6j, k and l). The spring rainfall patterns are similar to those observed using WFDE5 except for the high rainfall in Karakoram (KA), which is also observed for the summer and autumn. On an average, ARs contribute $25-30\%$ of rainfall in spring to northern IB and northwest GB (Figures S6i). In autumn, ARs contributed $10-15\%$ in most parts of GB with some grid cells showing 20% in the west and southmost (for rainfall of greater than 870 mm/autumn). In IB, AR contributes from 5% in the south to 40% in the foothills and KA. Overall, the rainfall patterns and relative contribution using IMD and WFDE5 are similar over both basins except for north IB.

Figure S7: Average Seasonal contribution of ARs using WFDE5.

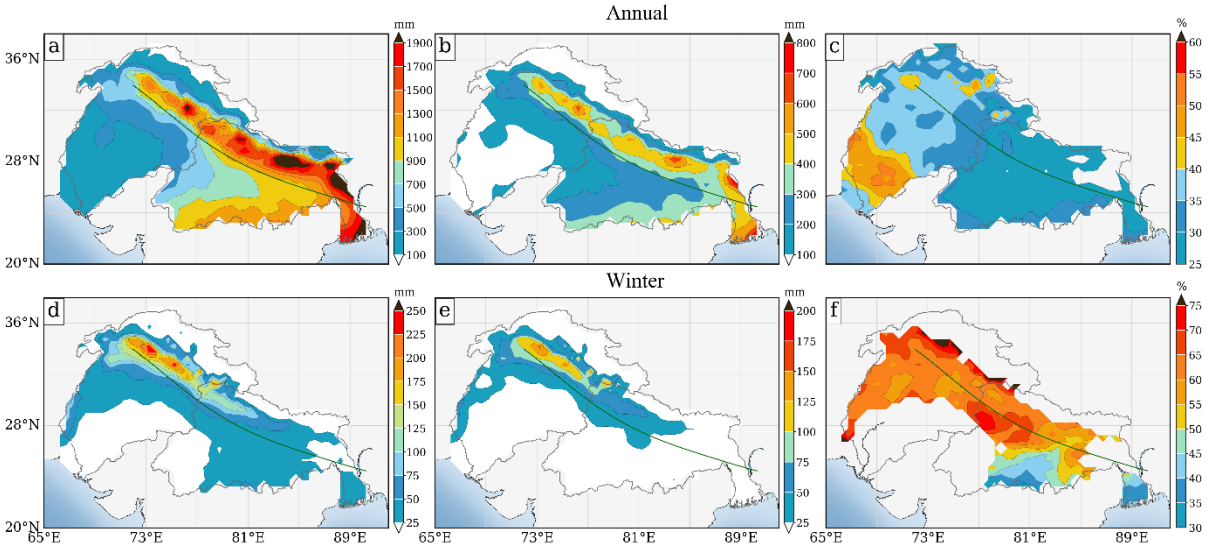

Figure S7a: Similar to Figures 2 and S6. [Note: those grids that have annual average less than 100mm and winter average (other seasons) less than 25 mm are not shown in the fractional contribution (white color)].

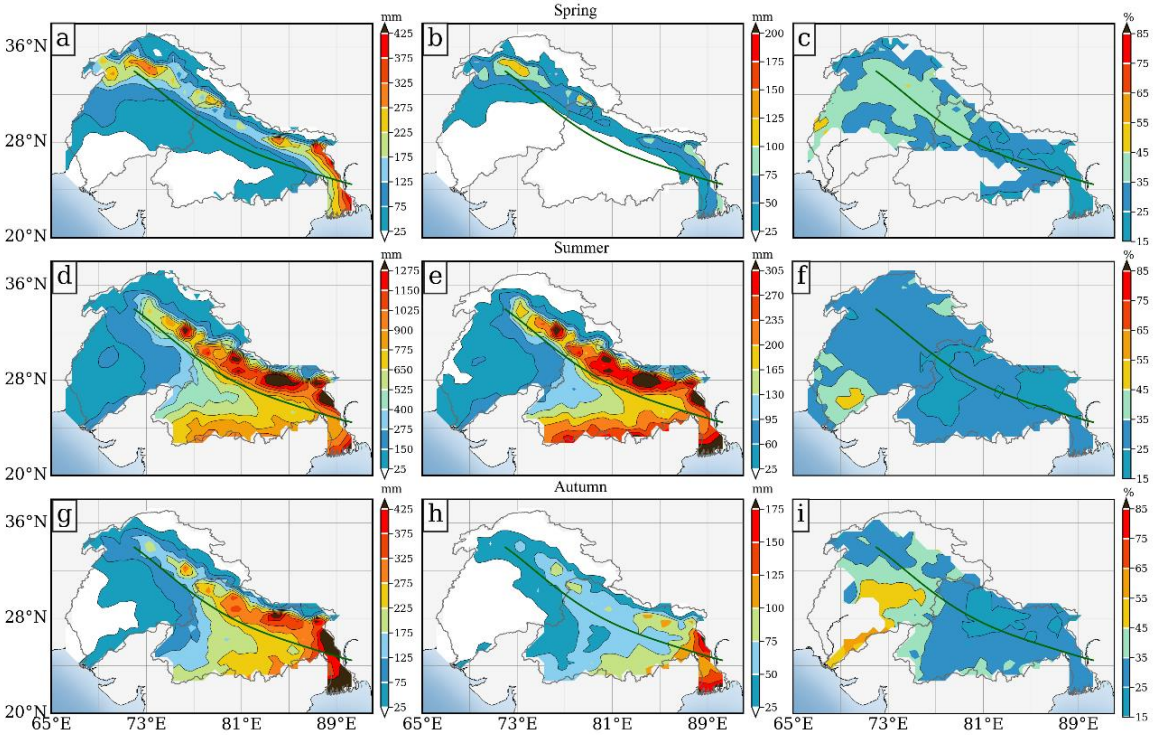

Figure S7b: Similar to Figures 2 and S7a. [Note: those grids that have annual average less than 25 mm are not shown in the fractional contribution (white color)].

Text S7a: Underestimation of AR fractional contributions:

The AR-related rainfall defined in this study and the resulting AR fractional contributions may be underestimated because (1) the method followed here does not consider grids close to the region within 250 km from the AR axis whose precipitation may be related

to ARs. This is for ARs with widths between $500 - 1000\ km$ (i.e., greater than the "250 km" considered here), (2) in the mountains, grids within 350 km that do not have IVT above the threshold (or slightly lower than the threshold) at any AR time step may have also not been included, as AR IVT is strongly depleted evolving to precipitation. We present the fractional contributions of ARs to rainfall in the two basins (Figures S7a and S7b) if we considered that precipitation on an AR day in either basin is related to AR, considering that ARs are large-scale features and due to large moisture divergences upon striking the mountain barrier, they can lead to precipitation at distances far from their major axes. We also include one day before and one day after the AR event without double counting the days between consecutive AR events (similarly followed for AR-derived snowfall by Huning et al., (2019), AR impacts on precipitation by Eldardiry et al., (2019) and hydrology by Leung & Qian, (2009) for western US and Viale et al., (2018) for southern South America). We observed that ARs contribute nearly 50% to the annual rainfall in the north IB and certain regions in lower IB (Figure S7c), and $25 - 35\%$ of the annual rainfall comes during ARs in GB, with higher fractions in the mountains (see Text S7b for more details).

Text S7b: Average Seasonal contribution of ARs using WFDE5:

On an average, AR contribute nearly 45% to the annual rainfall in the south IB and 40% in northern IB and between $30 - 35\%$ of the annual rainfall in GB comes during ARs (Figure S7a (c)). ARs have the highest contribution to rainfall in winter season, with $70 - 75\%$ of the rainfall is related to ARs in IB, and northwest GB and $35 - 45\%$ in south GB (Figure S7a (f)). On an average, ARs contribute $35 - 45\%$ of rainfall in spring to upper IB and northwest GB (Figures S7b (c)). ARs contribute nearly 30% of the summer rainfall in the IB except the south and in GB, ARs contribute $\sim 25 - 30\%$ of the seasonal summer rainfall (for rainfall between $625 - 1100$ mm/summer) in northern GB (Figures S7e and f). In autumn, ARs contributed $\sim 35\%$ in south GB and gradually the contribution decreases to 25% in north GB (CH), $25 - 50\%$ in the IB with higher fractions for precipitation below 125 mm/autumn. The relative contributions obtained using the method describe in Text S7a are comparatively higher.

Figure S8: Seasonal precipitation extremes using IMD

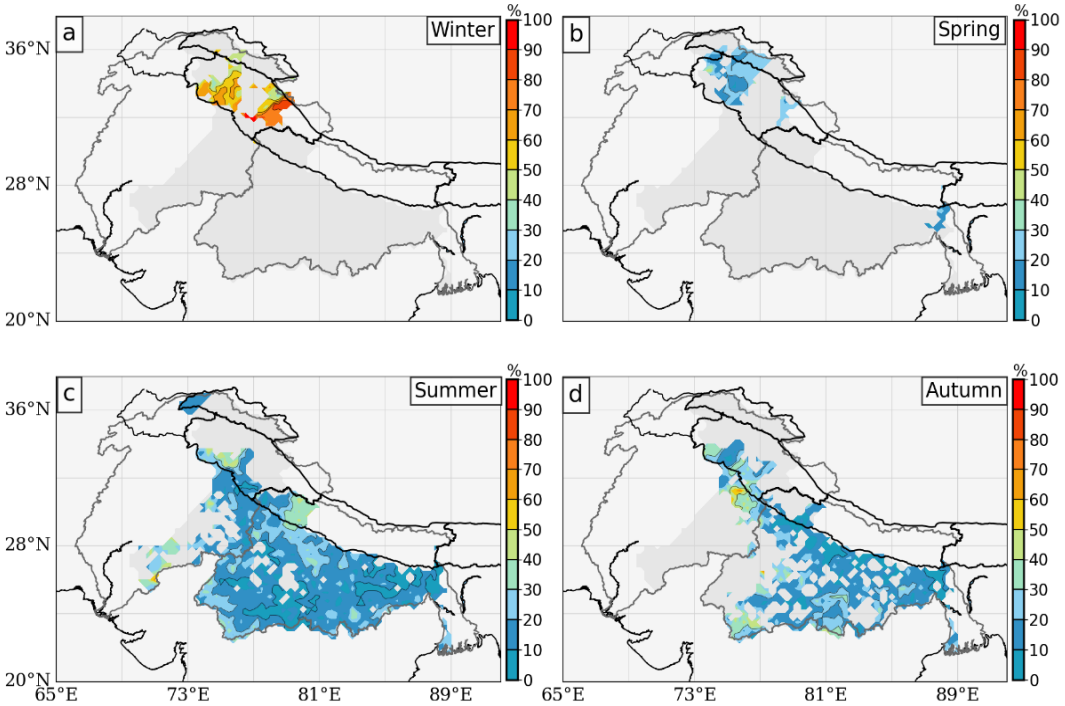

Figure S8a: Similar to Figure 5 using IMD. Relative frequency of seasonal rainfall maxima related to ARs for 1982 – 2018 (a) for winter, (b) spring (c) summer, and (d) autumn seasons. The grids shaded in grey have either seasonal maximum precipitation less than 60mm or the number of seasonal maxima is less than 7.

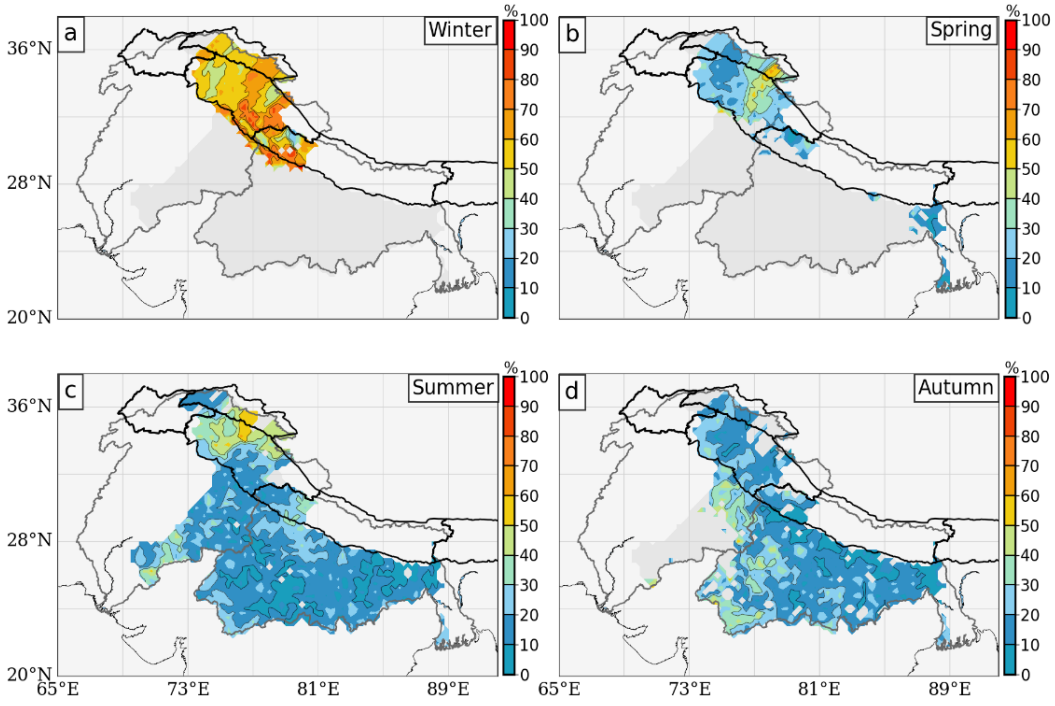

Figure S8b: Similar to Figure 5 using IMD. The criteria for seasonal maximum rainfall include (1) daily rainfall amount greater than 40mm and (2) the number of seasonal maxima is should be 7 or more.

Text S8: Seasonal precipitation extremes using IMD

In Figure S8a, over 50% of winter extremes are AR-related in the upper IB (WH and central KA). In GB, the winter maxima are very low (80th percentile varies between 20-50mm) to satisfy the conditions for extremes defined here. We observed similar results (over 50%) for spring extremes (Figure S8a (b)) and also noted $20-30\%$ of extremes in the east GB are AR-related. The gradual increase in contribution from west-east in the northern IB (WH and KA) corresponds to the gradual west-east increase in elevation where greater precipitation is extracted at higher altitudes (Neiman et al., 2008). In east IB, some grids have $\sim$50% of their spring extremes related to ARs, suggesting that intense ARs are capable to penetrate into the mountains. In summer, ARs are responsible for $50-70\%$ of extremes in upper IB (west of WH and central KA), and some regions in south IB, and less than 50% in rest of IB (Figure S8a (c)). In GB, AR contributions to summer and autumn extremes are generally weak. Higher fractions are found along the southern periphery and in the mountains (northwest) In IB, summer and autumn AR-related extremes are higher than in GB and mostly along the foothills of the WH as precipitation is mainly concentrated here during these seasons.

Figure S9: Location of flood events in IB and GB

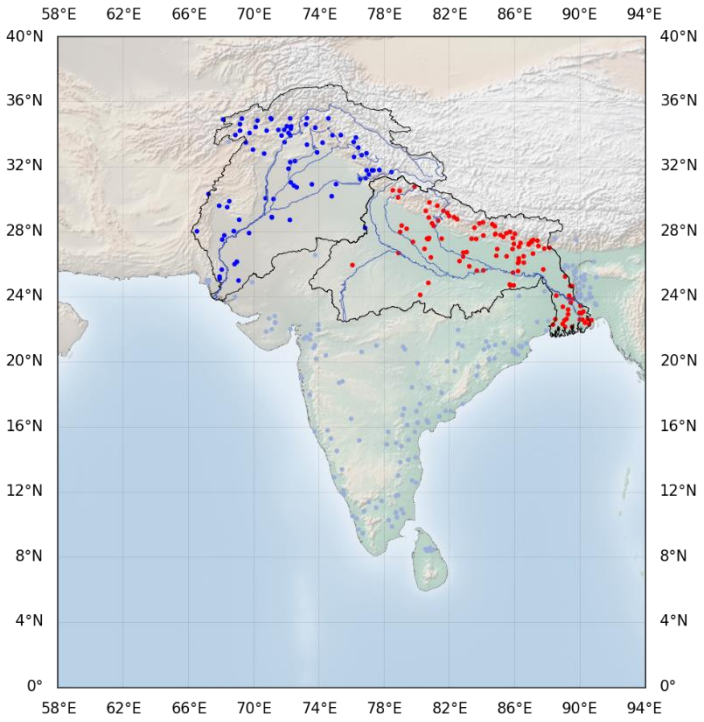

Figure S9: The dots represent the locations of the flood events during the period $1985-2018$ in IB (in blue) and in GB (in red). The grey colored dots are for other parts of India outside the study region.

Figure S10: Modified Lavers et al., (2012) versus Guan & Waliser, (2019) AR detection algorithms.

Figure S10a: A contingency table showing the number of AR days detected by Lavers et al., (2012) and Guan & Waliser, (2019) algorithms. The top left (ARs) and bottom right (no ARs) represents the days when both Lavers et al., (2012) and Guan & Waliser, (2019) algorithms agree, the top right shows the number of AR days that only Guan & Waliser, (2019) algorithm identified, and similarly the bottom left shows the number of AR days that are detected only by the Lavers et al., (2012) algorithm.

Here, we considered an AR day if any of the time steps have an AR. We then compared the dates in the two sets, as shown in Figure S9, and we found that 82% of the ARs from Nayak et al., (2021)) (using a modified Lavers et al., (2012)) match the ARs from the Guan & Waliser, (2019) algorithm , "tARget". Most of the AR events identified by "tARget" have short duration, existing less than a day, hence for the comparison we have included all the dates from GW19.

We have also shown the comparisons of the spatial patterns of average total and AR-related rainfall at annual and seasonal timescales below (Figure S9b, similar to Figure 2). We have followed the methods described in the main text to quantify AR-related rainfall for the ARs obtained from tARget.

A. Spatial patterns using the ARs from Nayak et al. (2021)

B. Spatial patterns using the ARs from Guan & Waliser, (2019)

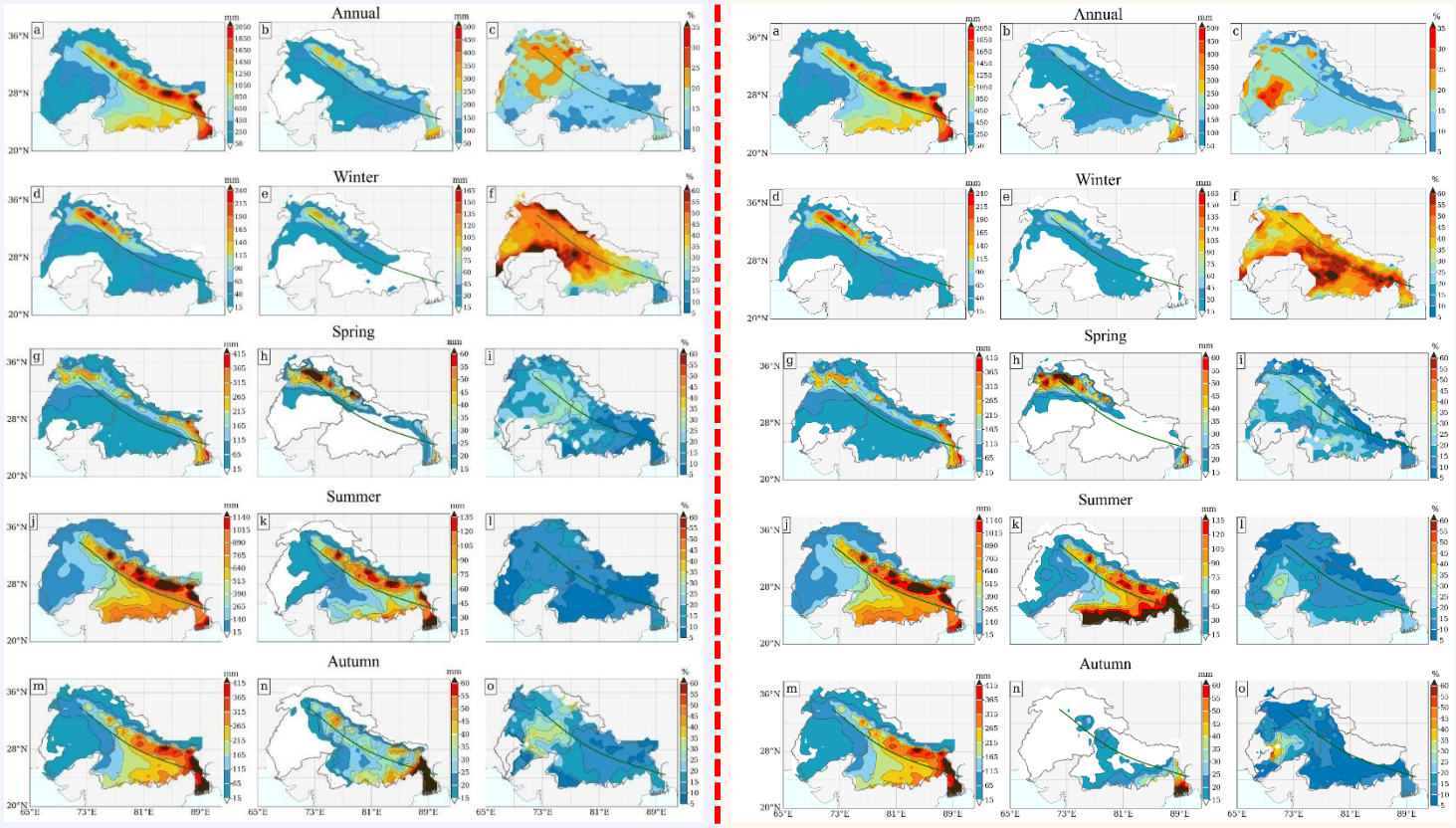

Figure S10b: Comparison of spatial rainfall patterns of AR-related and percent contribution of ARs to total (average) rainfall using ARs from Nayak et al. (2021) (Panel A) and Guan & Waliser, (2019) (Panel B): In each panel the spatial distribution of annual (seasonal) average is shown in first column [(a), (d), (g), (j), (m), units are mm/year or mm/season]; AR-related rainfall in second column [(b), (e), (h), (k), (n), units are in mm/year or mm/season]; and fractional contribution are shown in the third column [(c),(f), (i), (l), (o), units are in %], over the period 1982 – 2016 using WFDE5 [Note: grid cells with annual (seasonal) average precipitation < 50 mm (<15) mm are not shown in the fractional contribution (white color)].

In Figure S9b, the spatial distribution of AR-related rainfall from tARget (Guan & Waliser, 2019) ARs (Panel B) resembles the spatial distribution of AR-related rainfall estimated using Nayak et al. (2021) ARs (Panel A), though there are differences in the intensities in each season. Both algorithms showed an agreement on the percent contribution of ARs in Ganga Basin (GB), though a few more grids in the southeast showed slightly higher contribution when using the tARget algorithm. AR-related rainfall from both algorithms showed that the winter rainfall is mainly AR-rainfall [more than 60% comes from ARs, Panels A and B (f)]. In Panel B, a slightly higher AR contribution is observed in west IB and GB which is related to slightly more AR-related contributions in spring and summer [Panel B, (c), (i), and (l)]. Similarly, for the north and south of GB, there is increased contribution from ARs in winter and summer [Panel B, (f) and (l)], though this increase may be related to AR-cyclones and ARs identified by tARget that intersect the transect at the southeast GB. In autumn, the

contribution of AR-related rainfall is smaller [Panel B, (o)] due to the low number of ARs identified during this season, which is mainly related to the thresholds and AR criteria used in the algorithm.

The key reasons that contributed to the differences in ARs obtained from Nayak et al., (2021) and the tARget algorithm are as follows:

- tARget uses monthly thresholds that can vary from 85th to 95th, but not $\leq 100\ \mathrm{kg.\,m^{-1}.\,s^{-1}}$, while Nayak et al. (2021) uses daily 85th percentile values that can be $\leq 100\ \mathrm{kg.\,m^{-1}.\,s^{-1}}$ in some season. Thus, tARget extracts more ARs in summer, but lesser ARs in non-monsoon, particularly over Western Himalaya, Karakoram, and Hindu Kush.
- tARget produces many short-duration ARs (< 18 hr), while ARs from Lavers et al., 2012 approach and thus from Nayak et al. (2021) are all persistent (≥ 18 hr).
- tARget retains timesteps when ARs and cyclones co-occur, which may affect the AR-impacts quantification. In contrast, Nayak et al. (2021) removes all AR timesteps that have cyclones.

References:

Eldardiry, H., Mahmood, A., Chen, X., Hossain, F., Nijssen, B., & Lettenmaier, D. P. (2019). Atmospheric River–induced precipitation and snowpack during the western United States cold season. *Journal of Hydrometeorology*, *20*(4), 613–630. https://doi.org/10.1175/JHM-D-18-0228.1

Guan, B., & Waliser, D. E. (2019). Tracking Atmospheric Rivers globally: spatial distributions and temporal evolution of life cycle characteristics. *Journal of Geophysical Research: Atmospheres*, *124*(23), 12523–12552. https://doi.org/10.1029/2019JD031205

Huning, L. S., Guan, B., Waliser, D. E., & Lettenmaier, D. P. (2019). Sensitivity of seasonal snowfall attribution to Atmospheric Rivers and their reanalysis-based detection. *Geophysical Research Letters*, *46*(2), 794–803. https://doi.org/10.1029/2018GL080783

Lavers, D. A., Villarini, G., Allan, R. P., Wood, E. F., & Wade, A. J. (2012). The detection of Atmospheric Rivers in atmospheric reanalyses and their links to British winter floods and the large-scale climatic circulation. *Journal of Geophysical Research: Atmospheres*, *117*(D20). https://doi.org/10.1029/2012JD018027

Leung, L. R., & Qian, Y. (2009). Atmospheric Rivers induced heavy precipitation and flooding in the western U.S. simulated by the WRF regional climate model. *Geophysical Research Letters*, *36*(3). https://doi.org/10.1029/2008GL036445

Nayak, M. A., Azam, M. F., & Lyngwa, R. V. (2021). *ERA5-based database of Atmospheric Rivers over Himalayas* (preprint). https://doi.org/10.5194/essd-2020-397

Neiman, P. J., Ralph, F. M., Wick, G. A., Lundquist, J. D., & Dettinger, M. D. (2008). Meteorological characteristics and overland precipitation impacts of Atmospheric Rivers affecting the west coast of North America based on eight years of SSM/I satellite observations. *Journal of Hydrometeorology*, *9*(1), 22–47. https://doi.org/10.1175/2007JHM855.1

Pai, D. S., & Bhan, S. C. (2014). *Monsoon Report 2014. ESSO Document No.: ESSO/IMD/Synoptic Met./01(2015)/17*, (p. 219). India Meteorological Department. Retrieved from https://www.tropmet.res.in/~kolli/MOL/Monsoon/year2014/Monsoon-2014-NEW.pdf

Rajeevan, M., Bhate, J., Kale, J. D., & Lal, B. (2006). High resolution daily gridded rainfall data for the Indian region: Analysis of break and active monsoon spells. *Current Science*, *91*(3), 296–306.

Viale, M., Valenzuela, R., Garreaud, R. D., & Ralph, F. M. (2018). Impacts of Atmospheric Rivers on precipitation in Southern South America. *Journal of Hydrometeorology*, *19*(10), 1671–1687. https://doi.org/10.1175/JHM-D-18-0006.1